Electrochimica Acta 55 (2010) 857–864

Contents lists available at ScienceDirect

Electrochimica Acta

journal homepage: www.elsevier.com/locate/electacta

Enhanced activity and stability of Pt/C fuel cell anodes by the modification with ruthenium-oxide nanosheets

Takahiro Saida, Wataru Sugimoto *,[1], Yoshio Takasu [1]

Department of Fine Materials Engineering, Faculty of Textile Science and Technology, Shinshu University, 3-15-1 Tokida, Ueda 386-8567, Japan

ARTICLE INFO

Article history:
Received 21 March 2009
Received in revised form
16 September 2009
Accepted 17 September 2009
Available online 24 September 2009

Keywords:
Direct methanol fuel cell
CO oxidation
Platinum
Ruthenium oxide
Electrocatalyst
Nanosheet

ABSTRACT

Ruthenium-oxide nanosheet (RuO_2ns) crystallites with thickness less than 1 nm were prepared via chemical exfoliation of a layered potassium ruthenate and deposited onto carbon supported platinum (Pt/C) as a potential co-catalyst for fuel cell anode catalysts. The electrocatalytic activity towards carbon monoxide and methanol oxidation was studied at various temperatures for different RuO_2ns loadings. An increase in electrocatalytic activity was evidenced at temperatures above 40 °C, while little enhancement in activity was observed at room temperature. The RuO_2ns modified Pt/C catalyst with composition of RuO_2:Pt = 0.5:1 (molar ratio) exhibited the highest methanol oxidation activity. CO-stripping voltammetry revealed that RuO_2ns promotes oxidation of adsorbed CO on Pt. In addition to the enhanced initial activity, the RuO_2ns modified Pt/C catalyst exhibited improved stability compared to pristine Pt/C against consecutive potential cycling tests.

1. Introduction

Development of anode catalysts with higher tolerance to catalyst poison and better stability are major issues that must be resolved for wide-spread commercialization of direct methanol fuel cells for portable electronics and polymer electrolyte fuel cells operating on reformed fuel for residential applications. The carbon supported platinum–ruthenium system is considered as one of the most promising anode catalysts for such fuel cells [1]. Metallic Ru in the alloy catalyst is known to promote the oxidation of the carbon monoxide. Carbon monoxide strongly adsorbs on the active Pt sites, inhibiting successive reaction of the fuel. The promotional effect of Ru has been mainly discussed based on the so-called "bi-functional mechanism" [2] and/or "ligand effect" [3]. The bi-functional mechanism is based on the assumption that Ru supplies an oxygen source (Ru–OH_{ad}) promoting the oxidation of CO on adjacent Pt sites. The ligand effect assumes that the energy level of the metal catalyst is modified so that the binding strength with the metal and adsorbed CO is weakened, resulting in a reduction in overpotential for CO oxidation. The possibility that some nanostructured ruthenium oxides (expressed as RuO_xH_y or $RuO_2{\cdot}xH_2O$ in the literature) may act as co-catalysts have attracted interest and debate [4–18]. Several studies have suggested that the binary PtRu alloy structure is not a prerequisite for obtaining the highest activity, and partially oxidized ruthenium species (RuO_x) that are present in the PtRu/C catalysts may contribute to the anodic activity [4–6]. Enhancement in methanol oxidation activity has been reported for Pt–RuO_2 composite catalysts although the activity of such material is in general lower than that of PtRu alloy [7–14]. On the contrary, other studies have reported that ruthenium oxide is inactive for CO oxidation [15–18]. One reason for the apparent inconsistency in the reported literature may be due to the various forms of ruthenium oxide with different oxidation states and hydrous states having different electrochemical characteristics.

In terms of catalyst stability, Ru has been reported to be vulnerable to dissolution under long-term fuel cell operation, especially by voltage fluctuation due to repeated start up and shut down [19–22]. It is well known that crystalline RuO_2 has high electrochemical stability within the hydrogen and oxygen evolution region [23–30]. However, it has also been reported that hydrous ruthenium oxide containing Ru^{3+} is not stable in acidic electrolyte [30].

We have studied the electrochemical behavior of crystalline RuO_2 nanosheet (RuO_2ns) electrodes derived by chemical exfoliation of layered $K_{0.2}RuO_{2.1}$. The negatively charged RuO_2 nanosheets with sub-nanometer thickness are stabilized as a colloid by tetrabutylammonium counter ions [25]. Earlier, we communicated that the modification of Pt/C with RuO_2 nanosheets decreases the potential for CO and CH_3OH electro-oxidation at 60 °C [31]. In the case of alloy catalysts, it has been reported that the optimal

* Corresponding author. Tel.: +81 268 21 5455; fax: +81 268 21 5452.
E-mail address: wsugi@shinshu-u.ac.jp (W. Sugimoto).
[1] ISE member.

0013-4686/$ – see front matter © 2009 Elsevier Ltd. All rights reserved.
doi:10.1016/j.electacta.2009.09.052

alloy composition changes as a function of temperature; Ru-rich catalysts (Pt:Ru = 1:1) are more active at 60 °C while Pt-rich catalysts (Pt:Ru = 3:1) are more active at 25 °C [32–34]. Thus, it is essential that the activity at different temperatures with different co-catalyst loadings is studied. In this work, a systematic investigation of the CO and CH_3OH oxidation activity on RuO_2ns modified Pt/C (RuO_2ns–Pt/C) was conducted with various RuO_2 nanosheet content at temperatures ranging from 25 to 60 °C in order to further understand the effect of the RuO_2 nanosheet modification. In addition, the stability of RuO_2ns–Pt/C was compared with pristine Pt/C.

2. Experimental

An aqueous colloid containing exfoliated RuO_2 nanosheet crystallites was prepared following a procedure reported earlier [25]. First, layered $K_{0.2}RuO_{2.1}$ was obtained by solid-state reaction. The interlayer K^+ was exchanged with H^+ by acid treatment to obtain layered $H_{0.2}RuO_{2.1}$ (residual potassium K/Ru <0.05:1 [25]). Layered $H_{0.2}RuO_{2.1}$ was then reacted with 50% aqueous ethylamine to obtain an ethylammonium–ruthenate intercalation compound, $(C_2H_5NH_3)_{0.2}RuO_{2.1}$. The interlayer ethylammonium was subsequently ion-exchanged with tetrabutylammonium by reaction of the ethylammonium–ruthenate intercalation compound with 10% aqueous tetrabutylammonium hydroxide, yielding a tetrabutylammonium–ruthenate intercalation compound, $((C_4H_9)_4N)_{0.2}RuO_{2.1}$. The solid product was centrifugally collected (15,000 rpm). The tetrabutylammonium–ruthenate intercalation compound in a powder form was dispersed in distilled water and subjected to ultrasonification for 30 min and centrifuged at 2000 rpm. The colloidal supernatant, which contains the exfoliated RuO_2 nanosheets (RuO_2ns), was used for further investigation.

Carbon supported Pt (30 mass% Pt) was prepared by an impregnation method reported previously [35,36]. Vulcan XC-72R was mixed with $Pt(NO_2)_2(NH_3)_2$ dissolved in ethanol, and then allowed to dry at 60 °C to a powder state. The dried precursor was reduced in a tube furnace under flowing H_2(10%)–N_2(90%) gas for 2 h at 200 °C. Pt/C was suspended in distilled water and added into the RuO_2ns colloid and thoroughly mixed. The amount of Pt/C added to the RuO_2ns colloid was controlled so that the molar ratio of the additive was RuO_2:Pt = 1:1, 0.5:1 and 0.2:1. Reaction of Pt/C with the RuO_2ns could be realized by sedimentation. The final product, RuO_2ns modified Pt/C, was obtained by drying the mixture at 80 °C. The samples will be denoted as RuO_2ns(1.0)–Pt/C, RuO_2ns(0.5)–Pt/C, and RuO_2ns(0.2)–Pt/C, according to the amount of RuO_2 in the composite. For comparative reasons, RuO_2ns supported on carbon, RuO_2ns/C (10 mass% RuO_2), and PtRu/C (20 mass% Pt and 10 mass% Ru; Ru source $Ru(NO_3)_3$ dissolved in ethanol) were also prepared. The prepared PtRu/C catalyst shows activity comparable to values reported in the literature [18,32,37]. The metal ratio in the samples was analyzed by energy-dispersive X-ray spectroscopy (EDX) (EMAX-7000; Noran Instruments Voyager). The structure of the catalysts was characterized by X-ray diffraction (XRD, Rigaku RINT-2550 with monochromated Cu Kα radiation at 40 kV and 50 mA).

The working electrode was prepared by depositing 20 μL of a 2 g L^{-1} electrocatalyst ink dispersed in distilled water on a mirror-polished glassy carbon rod (40 μg-catalyst per 0.196 cm^2 exposed surface) with a micropipette. For electrochemical studies, the overall amount of catalyst was kept constant, giving metal loadings for the non-modified electrodes as 12 μg-metal for Pt/C and PtRu/C. For the RuO_2 nanosheet modified electrodes, the Pt loadings are 11.5, 10.9, and 10 μg-Pt cm^{-2} for RuO_2ns:Pt with 0.2, 0.5, and 1.0. 20 μL of a 1 wt% Nafion ionomer (resulting in a calculated Nafion thickness of ~4.5 μm) was dropped onto the electrode surface to immobilize the electrocatalysts. A beaker-type electrochemical cell equipped with the working electrode, a platinum mesh counter electrode and an Ag/AgCl/KCl (sat.) reference electrode, connected with a salt bridge, was used. A Luggin capillary faced the working electrode at a distance of 2 mm. Electrochemical measurements were conducted at 25, 30, 40, 50 and 60 °C. All electrode potentials throughout the paper will be referred to the reversible hydrogen electrode (RHE) scale corrected for the temperature effect (RHE(t)) according to the following equation:

$$E \text{ vs. RHE}(t) = E \text{ vs. Ag/AgCl} + (224 - T) \times \frac{\partial T}{\partial E} - \frac{RT}{nF} \times \text{pH} \times 2.303$$

where R is the gas constant (8.314 J K^{-1} mol^{-1}), T is the temperature, n is the number of electrons involved in the reaction (in this case, n = 1), F is the Faraday constant (96,485 C mol^{-1}) and $\partial T/\partial E$ is 0.0010 K V^{-1}.

Oxidation of pre-adsorbed carbon monoxide (CO_{ad}) was measured by CO_{ad} stripping voltammetry in 0.5 M H_2SO_4 at a scan rate of 10 mV s^{-1}. Gaseous CO(10%)–N_2(90%) was purged into the 0.5 M H_2SO_4 electrolyte for 90 min to allow complete adsorption of CO onto the catalyst surface while maintaining a constant voltage of 50 mV vs. RHE(t). Excess CO in the electrolyte was then purged out by bubbling N_2 gas for 40 min. The electrochemical surface area (ECSA) of the catalysts was calculated from the CO-stripping voltammograms. The amount of CO_{ad} was measured by integration of the CO_{ad} stripping peak, corrected for the electrical double-layer capacitance, assuming a monolayer of linearly adsorbed CO on metal surface and the Coulombic charge necessary for oxidation as 420 μC cm^{-2}. Electro-oxidation of CH_3OH was characterized by chronoamperometry at 500 mV in 0.5 M H_2SO_4 containing 1 M CH_3OH at various temperatures. The ECSA obtained from CO-stripping voltammetry was used to calculate the specific activity, i.e., the quasi-steady state current for methanol electro-oxidation obtained by chronoamperometry after 30 min of polarization normalized by the ECSA. The mass activity was obtained by normalizing the amount of Pt coated onto the glassy carbon surface. Catalyst stability was characterized by measuring the methanol oxidation activity after the catalysts were subjected to potential cycling. After the initial methanol oxidation activity was measured, the electrolyte was changed to a fresh 0.5 M H_2SO_4 electrolyte free of methanol. The potential was then cycled between 0.05 and 1.2 V at 50 mV s^{-1} for 1000 cycles at 60 °C. Methanol was then added into the electrolyte and the methanol oxidation activity was again measured by chronoamperometry.

3. Results and discussion

3.1. Structural characterization

Fig. 1(a) shows the XRD pattern of a film obtained by casting the RuO_2ns colloid. A series of (0 0 l) diffraction peaks typical of a well-ordered layered structure with an interlayer spacing of ~1.7 nm is observed. Thus, by casting the RuO_2ns colloid, re-stacking and re-organization of the exfoliated RuO_2ns occurs resulting in a tetrabutylammonium intercalation compound. The lack of such two-dimensional ordering for RuO_2ns(0.5)–Pt/C (Fig. 1(b)) is evidence that RuO_2ns is deposited onto the carbon surface with negligible re-stacking. Weak diffraction peaks at 2θ = 10° and 35° are observed, which is attributed to partial ordering of the RuO_2ns. The XRD peaks attributed to metallic Pt in RuO_2ns(0.5)–Pt/C are identical in peak position and width with Pt/C. Thus, the Pt particle size is not affected by the RuO_2ns modification and there is no atomic alloying of Ru into the Pt structure. This is anticipated since the RuO_2ns–Pt/C composite is not exposed to any heat treatment other than the drying process. The observed Ru:Pt ratio of the prepared catalyst as determined by energy-dispersive X-ray measurements was Ru:Pt = 0.92:1, 0.52:1, 0.15:1 for RuO_2ns(1.0)–Pt/C,

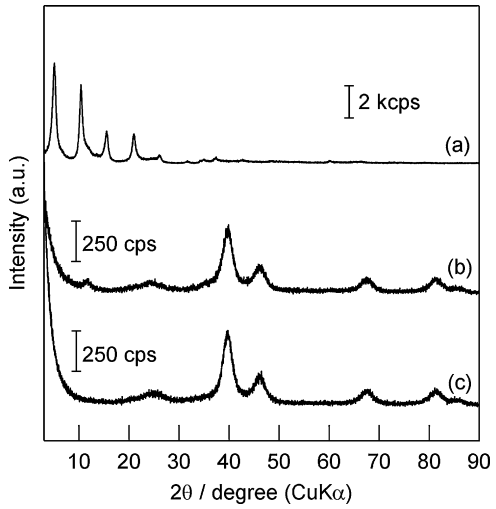

Fig. 1. The XRD patterns of (a) cast RuO_2ns film, (b) RuO_2ns(0.5)–Pt/C and (c) Pt/C.

RuO_2ns(0.5)–Pt/C, and RuO_2ns(0.2)–Pt/C, in agreement with the nominal content.

3.2. Electrochemical properties of RuO_2ns/C

The electrochemical properties of RuO_2ns/C (10 mass%) in the absence of Pt nanoparticles were first evaluated to understand the electrocatalytic activity of RuO_2ns alone. The cyclic voltammograms of RuO_2ns/C in 0.5 M H_2SO_4 at various temperatures are shown in Fig. 2. These voltammograms represent the background for the RuO_2ns–Pt/C composite. Three characteristic redox pairs are observed at ~0.1, 0.65 and 0.8 V (hereafter denoted A1/C1, A2/C2, A3/C3). A2/C2 and A3/C3 are attributed to electrosorption of anionic and cationic species, respectively [27,28]. A1/C1 is uncommon for polycrystalline RuO_2 systems but bears similarity to peaks observed in high quality RuO_2 (1 0 0) single crystal surfaces [38]. The A1/C1 pair is tentatively ascribed as adsorption/desorption of hydronium ions on the surface of the RuO_2ns, similar to that observed on RuO_2 (1 0 0) [38]. The specific capacitance of RuO_2ns/C, calculated by averaging the charge of the anodic and cathodic portion of the voltammograms, at 60 °C was ~73 F (g-catalyst)$^{-1}$ which translates to ~732 F (g-RuO_2)$^{-1}$ at 10 mV s^{-1}, comparable to the value of unsupported RuO_2ns.

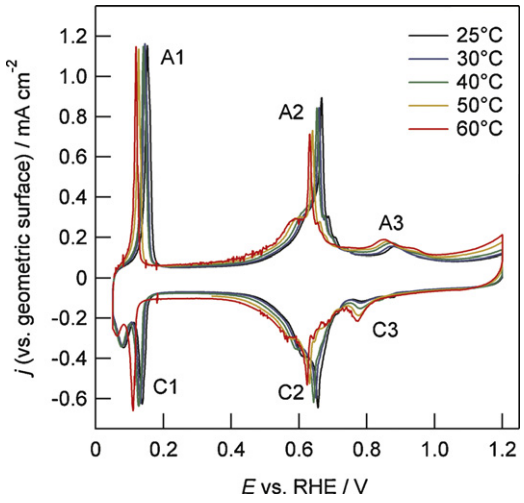

Fig. 2. Cyclic voltammograms of RuO_2ns/C at various temperatures in 0.5 M H_2SO_4 at $\nu = 10$ mV s^{-1}.

Table 1
Specific capacitance and electrochemically active Pt surface area (S_{ECA}) of RuO_2ns–Pt/C measured at 60 °C.

Sample	Specific capacitance (F (g-composite)$^{-1}$)	S_{ECA} (m^2 (g-Pt)$^{-1}$)
RuO_2ns(1.0)–Pt/C	199	83
RuO_2ns(0.5)–Pt/C	166	64
RuO_2ns(0.2)–Pt/C	147	71
Pt/C	97	52

Fig. 3 shows the CO_{ad} stripping voltammograms for RuO_2ns/C at various temperatures. It is clear that RuO_2ns behaves as a poor electrocatalyst for CO oxidation. The poor CO oxidation behavior of RuO_2ns can be attributed to the lack of CO adsorption sites on the RuO_2ns surface. Note that the A1/C1 peak is still evident after the CO adsorption procedure. If the A1/C1 peak was due to hydrogen desorption/adsorption similar to many metal surfaces, this peak is anticipated to disappear by the replacement of hydrogen with CO. As this is not the case, the A1/C1 peak is probably not due to hydrogen desorption/adsorption.

Voltammograms in 0.5 M H_2SO_4 + 1 M CH_3OH of RuO_2ns/C at various temperatures are shown in Fig. 4. There is essentially no difference between the voltammograms with and without CH_3OH in the electrolyte below ~1.0 V. Evidently, CH_3OH adsorption does not occur on the surface of RuO_2 nanosheets in the region of practical meaning to anode catalysts for fuel cells. The above results show that RuO_2ns single-handedly is a poor electrocatalyst for CO and CH_3OH oxidation.

3.3. CO tolerance of RuO_2ns–Pt/C with different RuO_2ns loadings

Cyclic voltammograms of RuO_2ns–Pt/C with various RuO_2ns content in 0.5 M H_2SO_4 (60 °C) are shown in Fig. 5. The CVs of RuO_2ns–Pt/C are characterized by features of both RuO_2ns/C and Pt/C. The A1/C1, A2/C2 and A3/C3 redox peaks distinctive of RuO_2ns can be clearly observed for all catalysts with different RuO_2ns loadings. The charge related with these redox peaks increases with increasing RuO_2ns content. The gravimetric capacitance also increases linearly with the RuO_2ns content (Table 1). The CO_{ad} stripping voltammograms of RuO_2ns–Pt/C with different RuO_2ns loadings at 60 °C are shown in Fig. 6. The onset and peak potential of CO_{ad} oxidation for RuO_2ns–Pt/C shows a negative shift compared to pure Pt/C. Although the CO tolerance of RuO_2ns–Pt/C is not good compared to PtRu/C, a gain of ~180 mV in the onset for CO_{ad} oxidation is observed by the modification of Pt/C with RuO_2ns. Since RuO_2ns itself is a poor CO oxidation catalyst, the enhanced CO_{ad} oxidation activity of RuO_2ns–Pt/C must be due to the ability of the RuO_2ns surface to supply an oxygen source (–OH) for the oxidation of CO_{ad} on the Pt surface. For RuO_2ns(0.2)–Pt/C, the promotional effect is seen only as a small shoulder peak on the negative potential side, and the potential for the main peak is more or less the same as Pt/C. For RuO_2ns(0.5)–Pt/C and RuO_2ns(1.0)–Pt/C, the shift in the onset potential of CO_{ad} oxidation is more clear. It should be emphasized that the main CO_{ad} oxidation peak is also shifted with regards to pure Pt ($E = 0.7$ V) for the catalysts with higher RuO_2ns content, i.e. RuO_2ns(0.5)–Pt/C and RuO_2ns(1.0)–Pt/C. The peak broadening and the shift in onset and peak potential observed for the higher loadings can be explained by the OH nucleation and diffusion on the RuO_2ns surface to nearby Pt sites. The reactions sites for CO_{ad} oxidation should be confined to sites where the RuO_2ns surface is in contact with the Pt surface. The broad and multiplex CO_{ad} oxidation peak can be interpreted as a result of the heterogeneous interface between RuO_2 nanosheets and Pt. Surface diffusion of OH groups on the RuO_2 nanosheet surface should be the main cause for the sluggish kinetics. The limited co-catalytic effect of RuO_2ns at low loading can be rationalized as insufficient contact between

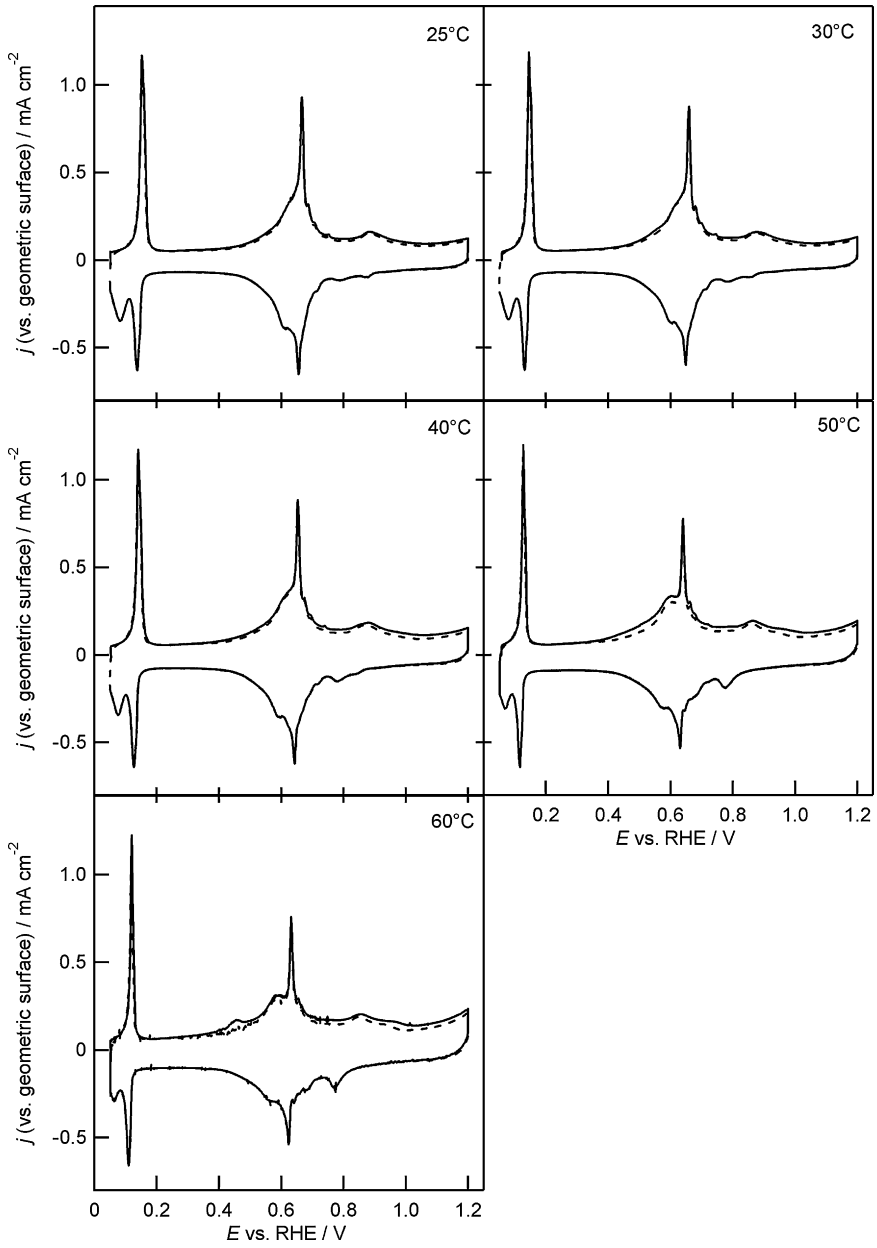

Fig. 3. CO_{ad} stripping voltammograms for RuO_2ns/C at various temperatures in 0.5 M H_2SO_4 at $\nu = 10$ mV s^{-1}. Solid line: 1st cycle after CO adsorption; broken line: 2nd cycle. Current normalized with respect to the geometric surface.

Pt nanoparticles and RuO_2ns. The sluggish CO oxidation kinetics of the RuO_2ns–Pt/C is similar to the behavior observed for Pt/RuO_2 catalysts. Surface diffusion of CO_{ad} has been shown to play a significant role in the CO oxidation reaction for Pt–Ru as well as Pt/RuO_2 catalysts [39]. As the Pt particle size for all the RuO_2ns–Pt/C catalysts is the same in this study, the CO oxidation kinetics most likely is governed by the OH nucleation and diffusion rate on the RuO_2ns surface.

Quantitative evaluation of the Pt surface area from the hydrogen adsorption/desorption peaks was not possible due to the overlapping of the A1/C1 redox peaks from RuO_2ns. The effective Pt surface area was thus estimated from the CO_{ad} oxidation charge. The electrochemically active Pt surface area (S_{ECA}) obtained from CO stripping is summarized in Table 1. Note that the S_{ECA} is a measure of only the electrochemically active Pt surface sites as CO does not adsorb on RuO_2ns. The modification with RuO_2ns induces an increase in S_{ECA}. RuO_2ns has a hydrophilic surface which may result in an increase in the interphase between the electrolyte and Pt nanoparticles.

Fig. 7 shows the effect of temperature on the CO_{ad} stripping voltammograms for RuO_2ns(0.5)–Pt/C, Pt/C and PtRu/C. The shape of the CO_{ad} oxidation peak for RuO_2ns(0.5)–Pt/C is strongly affected by the temperature. At 25 °C, the CO_{ad} stripping voltammogram of RuO_2ns(0.5)–Pt/C is similar to that of Pt/C, indicating that RuO_2ns does not promote CO_{ad} oxidation. The co-catalytic effect of RuO_2ns becomes obvious as the reaction temperature is increased, as evidenced by the gradual broadening and splitting of the CO_{ad} oxidation peak with increasing temperature. Although RuO_2ns acts as a promoting additive, it is not as effective as Ru in the PtRu alloy. Obviously, the Pt nanoparticles and RuO_2ns have limited contact compared to an intimately mixed PtRu alloy and an electronic effect is rather unlikely. However, the CO tolerance of RuO_2ns(1.0)–Pt/C is comparable to PtRu/C at elevated temperatures, where PtRu/C stability may become a major issue. The instability of Ru under the fuel

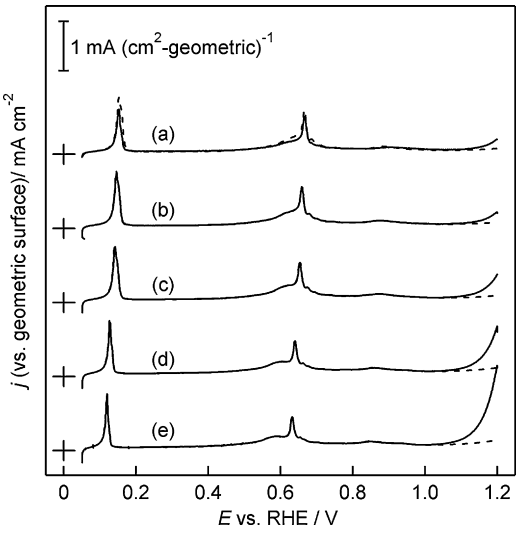

Fig. 4. Voltammograms of RuO_2ns/C at (a) 25 °C, (b) 30 °C, (c) 40 °C, (d) 50 °C and (e) 60 °C at $\nu = 10$ mV s^{-1}. Solid line: 0.5 M H_2SO_4 + 1 M CH_3OH; broken line: 0.5 M H_2SO_4. Current normalized with respect to the geometric surface.

cell operation conditions has been reported [20–22]. The amount of Ru loss due to dissolution should increase with increasing cell temperature.

3.4. CH_3OH oxidation activity of RuO_2ns–Pt/C

Chronoamperograms of RuO_2ns–Pt/C, Pt/C and PtRu/C catalysts in 0.5 M H_2SO_4 + 1 M CH_3OH (60 °C) are shown in Fig. 8. The mass and specific activities of methanol oxidation calculated from the quasi-steady state current after 30 min are summarized in Table 2. The specific activity (the current density normalized by the S_{ECA} of Pt obtained from CO-stripping voltammetry) for RuO_2(0.5)–Pt/C was almost as high as PtRu/C, and roughly 8 times higher than that of Pt/C. The mass activity for CH_3OH oxidation for RuO_2(0.5)–Pt/C and RuO_2(1.0)–Pt/C showed an enhancement of approximately 10 times compared to Pt/C. It is obvious that RuO_2ns acts as a co-catalyst for CH_3OH oxidation due to the enhanced CO_{ad} oxidation activity.

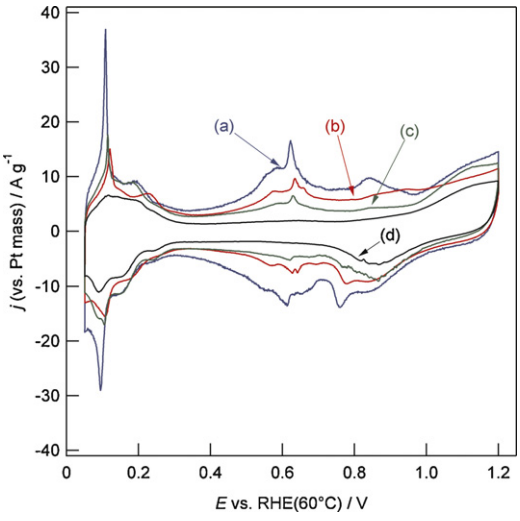

Fig. 5. Cyclic voltammograms of (a) RuO_2ns(1.0)–Pt/C, (b) RuO_2ns(0.5)–Pt/C, (c) RuO_2ns(0.2)–Pt/C, and (d) Pt/C in 0.5 M H_2SO_4 (60 °C) at $\nu = 10$ mV s^{-1}. Current normalized with respect to the Pt mass.

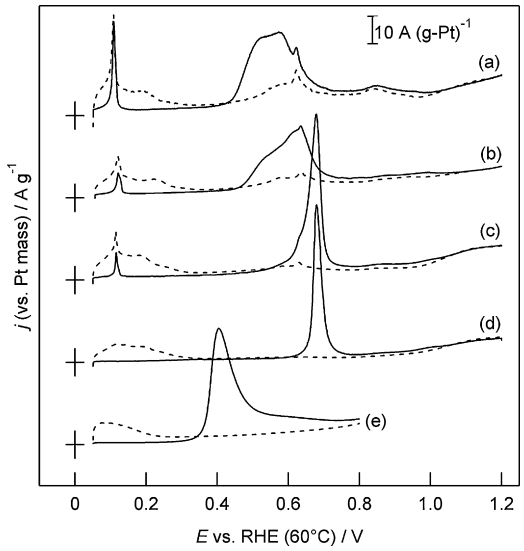

Fig. 6. CO_{ad} stripping voltammograms of (a) RuO_2ns(1.0)–Pt/C, (b) RuO_2ns(0.5)–Pt/C, (c) RuO_2ns(0.2)–Pt/C, (d) Pt/C and (e) PtRu/C in 0.5 M H_2SO_4 (60 °C) at $\nu = 10$ mV s^{-1}. Solid line: 1st cycle after CO adsorption; broken line: 2nd cycle. Current normalized with respect to the Pt mass.

The temperature dependence of the CH_3OH oxidation activity was studied for the RuO_2ns(0.5)–Pt/C catalyst. The voltammograms measured at various temperatures for RuO_2ns(0.5)–Pt/C are compared with Pt/C and PtRu/C in Fig. 9. The temperature dependence of CH_3OH oxidation follows a similar tendency to the CO_{ad} oxidation behavior, which is not surprising since CO poisoning occurs only on Pt sites as mentioned earlier. At elevated temperatures, the CH_3OH oxidation activity of RuO_2ns(0.5)–Pt/C catalyst is higher compared to Pt/C, but is slightly lower than that of PtRu/C. At ambient temperature, CH_3OH oxidation on RuO_2ns(0.5)–Pt/C is similar to that of Pt/C, since diffusion of OH_{ad} on RuO_2ns is not sufficient for the RuO_2ns to participate in the oxidation of the intermediate products. The temperature dependence of the mass activity obtained from chronoamperometry in 0.5 M H_2SO_4 + 1 M CH_3OH for RuO_2ns(0.5)–Pt/C, Pt/C and PtRu/C is shown in Fig. 10. The slope in the $\log j - T^{-1}$ curve for RuO_2ns(0.5)–Pt/C was larger compared to Pt/C and PtRu/C, showing the strong temperature dependence of the co-catalytic effect of RuO_2ns. The apparent activation energy E_a estimated from the slope in the $\log j - T^{-1}$ curve for RuO_2ns(0.5)–Pt/C was ~102 kJ mol^{-1}, while for Pt/C and PtRu/C E_a was ~53 and ~33 kJ mol^{-1}, respectively.

3.5. Stability of RuO_2ns(0.5)–Pt/C and Pt/C

It has been reported that metallic Ru in the PtRu alloy catalyst dissolves as Ru^{n+} and deposits at the cathode under fuel cell operating conditions, leading to catalyst degradation [20–22]. Thus, the stability of RuO_2ns(0.5)–Pt/C was considered by an accelerated stability test (potential cycling between 0.05 and 1.2 V vs. RHE in 0.5 M H_2SO_4(60 °C) at 50 mV s^{-1} for 1000 cycles). Fig. 11 compares cyclic

Table 2
Methanol oxidation activity of RuO_2ns–Pt/C, Pt/C and PtRu/C.

Sample	Mass activity (A (g-Pt)$^{-1}$)	Specific activity (A m^{-2})
RuO_2ns(1.0)–Pt/C	42	0.50
RuO_2ns(0.5)–Pt/C	47	0.73
RuO_2ns(0.2)–Pt/C	5	0.11
Pt/C	4	0.08
PtRu/C	83	0.78

Polarization potential: 500 mV vs. RHE; electrolyte: 0.5 M H_2SO_4 + 1 M CH_3OH (60 °C).

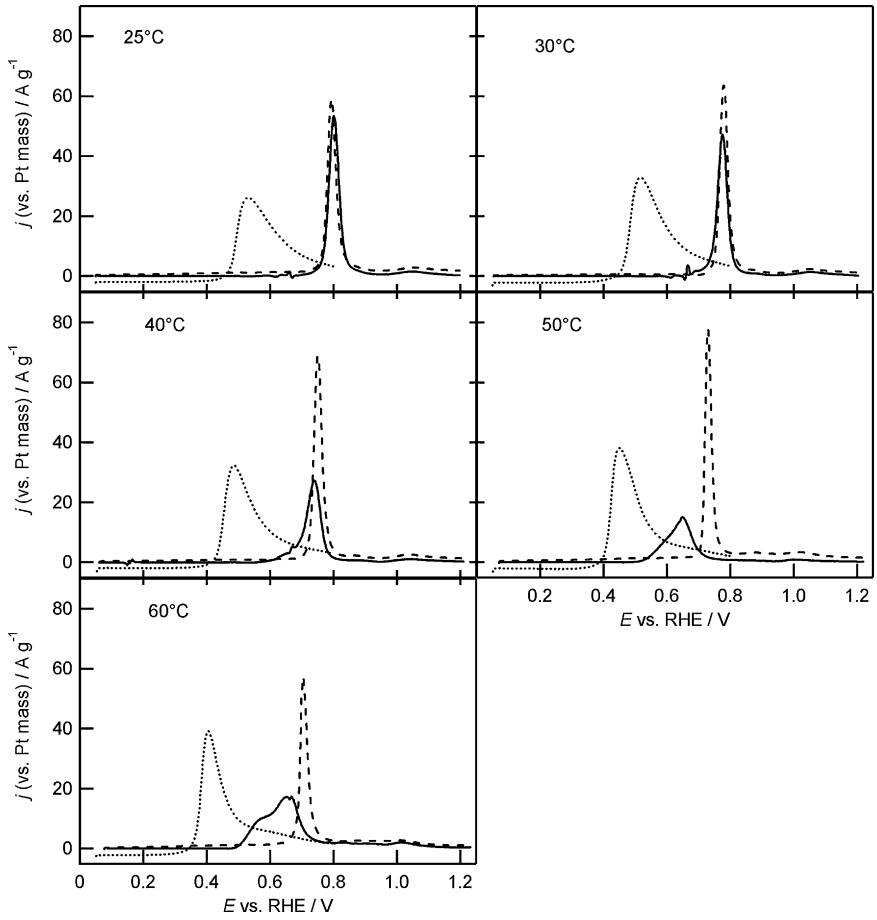

Fig. 7. CO_{ad} stripping voltammograms (difference spectra) for RuO_2ns(0.5)–Pt/C (solid line), Pt/C (broken line) and PtRu/C (dotted line) at various temperatures in 0.5 M H_2SO_4 at $\nu = 10$ mV s^{-1}. Current normalized with respect to the Pt mass.

voltammograms in 0.5 M H_2SO_4 (60 °C) for RuO_2ns(0.5)–Pt/C, Pt/C, and PtRu/C before and after the stability test. The results show that RuO_2ns is stable under conditions that PtRu would be drastically de-activated due to irreversible oxidation of Ru. The S_{ECA} obtained from the hydrogen adsorption current for Pt/C decreased drastically from S_{ECA} = 57 to 14 m^2 (g-Pt)$^{-1}$ after the stability test. In the case of RuO_2ns(0.5)–Pt/C, the S_{ECA} decreased only 55% in comparison with initial state, showing that the presence of RuO_2ns increases the stability of Pt nanoparticles. After the accelerated potential cycling test, the methanol oxidation activity of Pt/C retained only

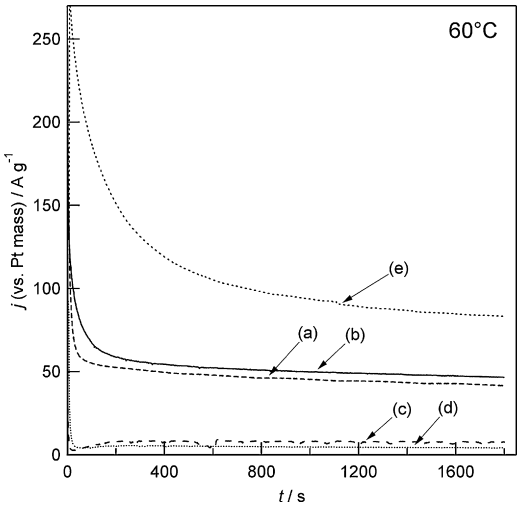

Fig. 8. Chronoamperometry curves for (a) RuO_2ns(1.0)–Pt/C, (b) RuO_2ns(0.5)–Pt/C, (c) RuO_2ns(0.2)–Pt/C, (d) Pt/C, and (e) PtRu/C in 0.5 M H_2SO_4 + 1 M CH_3OH (60 °C) at E = 0.5 V vs. RHE. Current normalized with respect to the Pt mass.

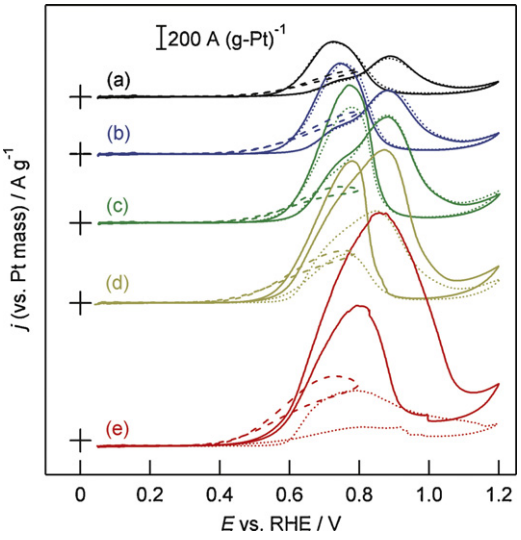

Fig. 9. Voltammograms of RuO_2ns(0.5)–Pt/C (solid line), Pt/C (dotted line) and PtRu/C (broken line) at (a) 25 °C, (b) 30 °C, (c) 40 °C, (d) 50 °C and (e) 60 °C in 0.5 M H_2SO_4 + 1 M CH_3OH at $\nu = 10$ mV s^{-1}. Current normalized with respect to the Pt mass.

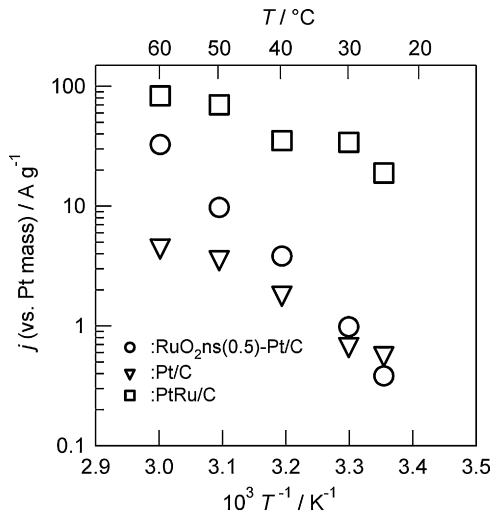

Fig. 10. The mass activities of RuO_2ns(0.5)–Pt/C (circles), Pt/C (triangles) and PtRu/C (squares) at 30 min after the potential step to 0.5 V vs. RHE in 0.5 M H_2SO_4 + 1 M CH_3OH at various temperatures. Current normalized with respect to the Pt mass.

~14% of its initial activity, decreasing from 7 to 1 A $(g\text{-Pt})^{-1}$. Under the same stability test conditions, the methanol oxidation activity of RuO_2ns(0.5)–Pt/C was 20 A $(g\text{-Pt})^{-1}$. Thus ~70% of the initial mass activity was maintained. The accelerated test conducted in this study is considerably intense bearing in mind that the anode potential of a fuel cell will not exceed 0.5 V in general. However, the results show that both activity and stability of Pt/C were dramatically increased by modification with RuO_2ns under the present experimental conditions. The role of RuO_2ns towards the enhanced stability must be studied in more detail in order to reach a sound conclusion. A tentative explanation is given on the basis of the strong acidic nature of RuO_2ns. RuO_2ns is intrinsically negatively charged ($[RuO_{2.1}]^{0.2-}$) and behaves as a solid acid, as indicated by the intercalation behavior of layered $H_{0.2}RuO_{2.1}$. Thus RuO_2ns should attract dissolved cationic Pt^{n+}, thereby acting as a protective layer inhibiting the diffusion of Pt^{n+} into the electrolyte.

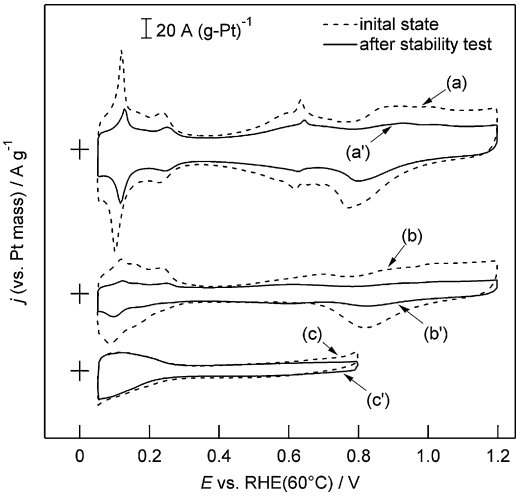

Fig. 11. Cyclic voltammograms of (a, a′) RuO_2ns(0.5)–Pt/C, (b, b′) Pt/C and (c, c′) PtRu/C before and after the stability test: (a) initial state of RuO_2ns(0.5)–Pt/C, (a′) after stability test of RuO_2ns(0.5)–Pt/C, (b) initial state of Pt/C, (b′) after stability test of Pt/C, (c) initial state of PtRu/C, (c′) after stability test of PtRu/C. Consecutive cycling test conditions: potential cycling between 0.05 and 1.2 V vs. RHE for 1000 cycles at 50 mV s^{-1} in 0.5 M H_2SO_4 (60 °C). Current normalized with respect to the Pt mass.

4. Conclusions

We have shown that high methanol oxidation activity is achieved by modifying conventional Pt/C with crystalline RuO_2 nanosheets (RuO_2ns). The highest activity was obtained for RuO_2ns–Pt/C with RuO_2:Pt = 0.5:1 (molar ratio) with a 10-fold increase in activity for methanol oxidation at 500 mV vs. RHE (60 °C). The increased activity is attributed to the co-catalytic effect of RuO_2ns towards CO_{ad} oxidation. The promotional effect is evident at temperatures above 40 °C, exhibiting a merit of ~180 mV for CO_{ad} oxidation. At room temperature, RuO_2ns does not promote CO_{ad} oxidation, most likely due to the poor kinetics of OH surface diffusion on RuO_2ns. Accelerated potential cycling tests indicated that the stability of RuO_2ns–Pt/C is drastically enhanced compared to Pt/C, which has been tentatively attributed to the solid acid characteristic of RuO_2ns, restraining the diffusion of Pt^{n+} into the electrolyte. RuO_2ns is an efficient co-catalyst exhibiting enhanced CO tolerance and improved catalyst stability.

Acknowledgments

The authors are grateful to Ishifuku Metal Industry Co., for kindly supplying $Pt(NH_3)_2(NO_2)_2$. This work was supported in part by a Grant-in-Aid for Scientific Research No. 18685026 and a Global COE Program by the Ministry of Education, Culture, Sports, Science, and Technology.

References

[1] E. Antolini, Mater. Chem. Phys. 78 (2003) 563.
[2] M. Watanabe, M. Motoo, J. Electroanal. Chem. 60 (1975) 267.
[3] T. Frelink, W. Visscher, J.A.R. van Veen, Surf. Sci. 335 (1995) 353.
[4] D.R. Rolison, P.L. Hangans, K.E. Swider-Lyons, J.W. Long, Langmuir 15 (1999) 774.
[5] J.W. Long, R.M. Stroud, K.E. Swider-Lyons, D.R. Rolison, J. Phys. Chem. B 104 (2000) 9772.
[6] B.J. Goodenough, A. Hamnett, B.J. Kennedy, R. Manoharan, S.A. Weeks, J. Electroanal. Chem. 240 (1988) 133.
[7] K. Lasch, G. Hayn, L. Jörissen, J. Garche, O. Besenhardt, J. Power Sources 105 (2002) 305.
[8] K. Lasch, L. Jörissen, K.A. Friedrich, J. Garche, J. Solid State Electrochem. 7 (2003) 619.
[9] Z. Chen, X. Qiu, B. Lu, S. Zhang, W. Zhu, L. Chen, Electrochem. Commun. 7 (2005) 593.
[10] H.M. Villullas, F.I. Mattos-Costa, L.O.S. Bulhões, J. Phys. Chem. B 108 (2004) 12898.
[11] H.B. Suffredini, V. Tricoli, L.A. Avsca, N. Vatistas, Electrochem. Commun. 6 (2004) 1025.
[12] L. Cao, F. Scheiba, C. Roth, F. Schweiger, C. Cremers, U. Stimming, H. Fuess, L. Chen, W. Zhu, X. Qiu, Angew. Chem. Int. Ed. 45 (2006) 5315.
[13] F. Scheiba, M. Scholz, L. Cao, R. Schafranek, C. Roth, C. Cremers, X. Qiu, U. Stimming, H. Fuess, Fuel Cells 6 (2006) 439.
[14] Z.-G. Shao, F. Zhu, W.-F. Lin, P.A. Christensen, H. Zhang, J. Power Sources 161 (2006) 813.
[15] A.H.C. Sirk, J.M. Hill, S.K.Y. Kung, V.I. Birss, J. Phys. Chem. B 108 (2004) 689.
[16] H. Hoster, T. Iwashita, H. Baumgärtner, W. Vilestich, J. Electrochem. Soc. 148 (2001) A496.
[17] W.E. O'Grady, P.L. Hagans, K.I. Pandya, D.L. Maricle, Langmuir 17 (2001) 3047.
[18] G. Wu, L. Li, B. Xu, Electrochim. Acta 50 (2004) 1.
[19] J.G. Liu, Z.H. Zhou, X.S. Zhao, Q. Xin, G.Q. Sun, B.L. Yi, Phys. Chem. Chem. Phys. 6 (2004) 134.
[20] P. Piela, C. Eickes, E. Brosha, F. Garzon, P. Zelenay, J. Electrochem. Soc. 151 (2004) A2053.
[21] A. Taniguchi, T. Akita, K. Yasuda, Y. Miyazaki, J. Power Sources 130 (2004) 42.
[22] Y. Chung, C. Park, G. -Su Park, W.S. Jeon, J.-R. Kim, Y. Lee, H. Chang, D. Seung, J. Phys. Chem. C 112 (2008) 313.
[23] J.P. Zheng, T.R. Jow, J. Electrochem. Soc. 142 (1995) L6.
[24] J.P. Zheng, P.J. Cygan, T.R. Jow, J. Electrochem. Soc. 142 (1995) 2699.
[25] W. Sugimoto, H. Iwata, Y. Yasunaga, Y. Murakami, Y. Takasu, Angew. Chem. Int. Ed. 42 (2003) 4092.
[26] W. Sugimoto, T. Kizaki, K. Yokoshima, Y. Murakami, Y. Takasu, Electrochim. Acta 49 (2004) 313.
[27] W. Sugimoto, H. Iwata, Y. Yasunaga, Y. Murakami, Y. Takasu, J. Electrochem. Soc. 151 (2004) A1181.
[28] W. Sugimoto, T. Ohta, K. Yokoshima, Y. Takasu, Electrochemistry 75 (2007) 645.
[29] W. Sugimoto, H. Iwata, K. Yokoshima, Y. Murakami, Y. Takasu, J. Phys. Chem. B 109 (2005) 7330.

[30] K.-H. Chang, C.C. Hu, J. Electrochem. Soc. 151 (2004) A958.
[31] W. Sugimoto, T. Saida, Y. Takasu, Electrochem. Commun. 8 (2006) 411.
[32] A.J. Dickinson, L.P.L. Carrette, J.A. Collins, K.A. Friedrich, U. Stimming, J. Appl. Electrochem. 34 (2004) 975.
[33] H.A. Gasteiger, N. Markovic, P.N. Ross Jr., E.J. Cairns, J. Electrochem. Soc. 141 (1994) 1795.
[34] A.S. Aricò, V. Baglio, A.D. Blasi, E. Modica, P.L. Antonucci, V. Antonucci, J. Electroanal. Chem. 557 (2003) 167.
[35] Y. Takasu, T. Fujiwara, Y. Murakami, K. Sasaki, M. Oguri, T. Asaki, W. Sugimoto, J. Electrochem. Soc. 147 (2000) 4421.
[36] Y. Takasu, H. Itaya, T. Kawaguchi, W. Sugimoto, Y. Murakami, Stud. Surf. Sci. Catal. 145 (2003) 279.
[37] T.J. Schmidt, H.A. Gasteiger, R.J. Behm, Electrochem. Commun. 1 (1999) 1.
[38] T.E. Lister, Y. Chu, W. Cullen, H. You, R.M. Yonco, J.F. Mithchell, Z. Nagy, J. Electroanal. Chem. 524–525 (2002) 201.
[39] C. Bock, M.-A. Blakely, B. MacDougall, Electrochim. Acta 50 (2005) 2401.